PERGAMON

International Journal of Heat and Mass Transfer 43 (2000) 3209–3217

International Journal of HEAT and MASS TRANSFER

www.elsevier.com/locate/ijhmt

Unsteady heat and mass transfer on the codeposition of SiO_2/GeO_2 during the modified chemical vapor deposition process

K.S. Park [a, 1], M. Choi [a, b,*], J.D. Chung [a, b]

[a] *School of Mechanical and Aerospace Engineering, Seoul National University, Seoul 151-742, South Korea*
[b] *National CRI Center for Nano Particle Control, Institute of Advanced Machinery and Design, Seoul, South Korea*

Received 30 April 1999; received in revised form 3 September 1999

Abstract

A numerical analysis of unsteady heat and mass transfer on the codeposition of SiO_2 and GeO_2 in the modified chemical vapor deposition has been carried out. An earlier study showed that the optimized torch speed variation could be used to enhance the deposition uniformity of single component SiO_2 particle. However, this optimized torch speed resulted in the deterioration of GeO_2 deposition uniformity for multi-component SiO_2/GeO_2 deposition in the present study. To ensure the uniformity of both SiO_2 and GeO_2, a control strategy may need variations of two parameters at least. Parametric studies, varying three different operating conditions over time (maximum wall temperature, torch speed and in-take amount of $GeCl_4$), reveals that the uniformity of SiO_2 deposition can be maintained by torch speed variation and that of GeO_2 can be obtained by increasing the in-take flow rate of $GeCl_4$ over time.

1. Introduction

The modified chemical vapor deposition (MCVD) process is utilized to manufacture high-quality optical fibers [1]. In the process, a fire polished silica tube is rotated and heated by a slowly traversing oxy-hydrogen torch. A mixture of gases, such as silicon tetrachloride ($SiCl_4$), germanium tetrachloride ($GeCl_4$), and oxygen (O_2) flow into the rotating silica tube and are heated to high temperatures. Chemical reactions occur and result in fine particles; e.g. silicon dioxide (SiO_2), germanium dioxide (GeO_2). These particles move axially with the gases and are deposited on the inner wall of the tube due to thermophoresis; that is, from the net force that a suspended particle experiences in the direction of decreasing temperature in a nonisothermal medium [2]. The deposited particles are consolidated into a glassy thin layer by sintering. When the torch completes its traverse to the end of the tube, one layer of deposition is obtained. By controlling the dopant chemical composition, desired refractive index profile is obtained. Germanium is the most common dopant used to increase the refractive index of SiO_2 to form a guiding core. After 10–40 layers are deposited, the tube is collapsed into a solid preform rod and then drawn into a long thin fiber.

The high-temperature chemical reactions, deposition and consolidation steps are interrelated and are

* Corresponding author. Tel.: +82-2-880-7128; fax: +82-2-883-0179.
E-mail address: mchoi@plaza.snu.ac.kr (M. Choi).
[1] Present address: LG Cable Inc.

0017-9310/00/$ - see front matter
PII: S0017-9310(99)00352-X

Nomenclature

C	gas concentration (mol m^{-3})
C_p	specific heat of gas at constant pressure (J mol^{-1} K^{-1})
D_i	diffusivity (m^2 s^{-1})
E_i	activation energy for oxidation (J mol^{-1})
ΔH_i	heat of reaction of species i (J mol^{-1})
h	heat transfer coefficient (W m^{-2} K^{-1})
k	thermal conductivity (J m^{-1} K^{-1} s^{-1})
$k_{GC,0}$	frequency factor for $GeCl_4$ oxidation (s^{-1})
k_{GC}, $k_{SC,0}$, $k_{SC,1}$	constants for oxidation reaction
k_0, k_1, k_2	constants to calculate thermal conductivity
K	thermophoretic coefficient
K_{EQ}	equilibrium constant of $GeCl_4$ oxidation
M	molecular weight
n	refractive index
n_i	moles of i species particles per mole of carrier gas
p	pressure
q_{max}	control parameter for torch heat flux
r	radial coordinate
r_i	rate of formation of particle i (GeO_2, SiO_2) by oxidation (m^{-3} s^{-1})
R_i	inner tube radius
R_G	gas constant
R_o	outer tube radius
S_i	source term in Eq. (6)
T	temperature (K)
t	time
u	radial velocity
v	axial velocity
$\vec{V}$	velocity (u, v)
$\vec{V}_T$	thermophoretic velocity of particles (m s^{-1})
X_i	mole fraction in the gas phase
x	axial coordinate
Y_i	mole fraction in the particle phase

Greek symbols

α	absorption coefficient
δm_i	deposition mass of particle i (GeO_2, SiO_2) per unit area
γ	activity coefficient of GeO_2 in GeO_2/SiO_2 particle phase
ε	emissivity
λ	control parameter for torch heat flux
ν	kinematic viscosity (m^2 s^{-1})
ρ	density
σ	Stefan–Boltzmann constant

Subscripts

CL	Cl_2
GC	$GeCl_4$
GO	GeO_2
O2	O_2
SC	$SiCl_4$
SO	SiO_2
0	inlet condition

affected by the details of thermal processing and control, as well as by the specific chemical mixture used. Thus, most previous studies of the MCVD have been numerical analyses. The previous investigations focused on various aspects of the problems: thermophoresis [2], correlation between overall efficiency and minimum temperature [3], laser-enhanced MCVD [4,5], chemical kinetics and silica aerosol dynamics [6], tapered entry region reduction [7,8], three-dimensional effect [9,10], codeposition of SiO_2 and GeO_2 [11], two torch model [12], oxidation of $SiCl_4$ and $GeCl_4$ and buoyancy [13], measurement of deposited film thickness and tube wall temperature [14]. However, there has been relatively little attention on the processing control for the optimum performance such as tapered entry region reduction and uniform deposition thickness. The reason of intactness in the control of the processing conditions may be found on the quasi-steady assumption used in previous works. Recently, Park and Choi [15] extended their work to the unsteady analysis and found out that unsteady calculations significantly improved the prediction of SiO_2 particle deposition profile in the entire region by comparing their results with the existing experimental study. They also examined the effects of torch speed variation on deposition performance for silica particles and identified that the linearly varying torch speed case resulted in a much shorter tapered entry than the constant torch speed case. For the codeposition of silica and germanium dioxide, very precise compositional and processing control is necessary to ensure the desired refractive index structures, especially for

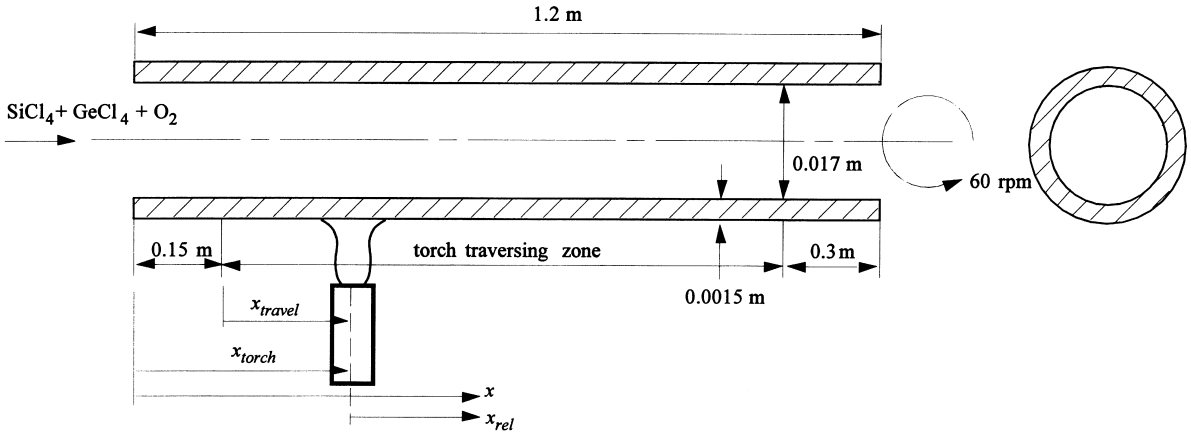

Fig. 1. Schematic diagram of the MCVD system.

multi-mode fiber manufacture, and optimum operating conditions will be considerably different from single component particle generation and deposition. Therefore, time dependent operating conditions such as torch speed, chemical gas flow rate and tube wall temperatures, etc. should be considered and, correspondingly, the unsteady analysis is prerequisite in its modeling.

In this paper, we extend our earlier work [15] to the unsteady analysis of multi-component (SiO_2 and GeO_2) MCVD. For the present unsteady calculation, the quartz tube is included in the calculation domain and the effects of chemical reactions for oxidations of both $SiCl_4$ and $GeCl_4$ and variable properties are also included. The time dependent operating conditions for the reduction of tapered entry and uniform deposition of both SiO_2 and GeO_2 are also examined.

2. Analysis

Fig. 1 depicts the geometric configuration considered in this study. A mixture of reactants ($SiCl_4$, $GeCl_4$ and O_2) is fed into a silica tube (reactor) as a fully developed laminar flow at the inlet. The mixture is heated by an external heat source and exothermic oxidations of $SiCl_4$ and $GeCl_4$ take place forming SiO_2, GeO_2 and Cl_2. From previous studies on the oxidation chemistry of $SiCl_4$ and $GeCl_4$ [16,17], it is well known that $SiCl_4$ oxidizes to form SiO_2 and its reverse reaction can be neglected, but the reverse and forward reaction of $GeCl_4$ oxidation should be considered:

$$SiCl_4+O_2 \rightarrow SiO_2+2Cl_2, GeCl_4+O_2 \leftrightarrow GeO_2+2Cl_2 \quad (1)$$

Fractions of newly formed silica and germanium dioxide particles are deposited onto the relatively low-temperature tube wall mostly by thermophoresis, while the rest exit the tube by convection.

Since uniform deposition in the circumferential direction can be assumed for normal rotational speeds (60–120 rpm) [10], the axisymmetric, two-dimensional unsteady governing equations can be written as

Continuity equation

$$\frac{\partial C}{\partial t}+\frac{1}{r}\frac{\partial}{\partial r}(Crv)+\frac{\partial}{\partial x}(Cu)=0 \quad (2)$$

Momentum equation

$$C\left(\frac{\partial u}{\partial t}+v\frac{\partial u}{\partial r}+u\frac{\partial u}{\partial x}\right) = -\frac{1}{M}\frac{\partial p}{\partial x}+\frac{1}{M}\left[\frac{2}{3}\frac{\partial}{\partial x}\left\{\mu\left(2\frac{\partial u}{\partial x}-\frac{\partial v}{\partial r}-\frac{v}{r}\right)\right\} + \frac{1}{r}\frac{\partial}{\partial r}\left\{\mu r\left(\frac{\partial u}{\partial r}+\frac{\partial v}{\partial x}\right)\right\}\right] \quad (3a)$$

$$C\left(\frac{\partial v}{\partial t}+v\frac{\partial v}{\partial r}+u\frac{\partial v}{\partial x}\right) = -\frac{1}{M}\frac{\partial p}{\partial r}+\frac{1}{M}\left[\frac{\partial}{\partial x}\left\{\mu\left(\frac{\partial u}{\partial r}+\frac{\partial v}{\partial x}\right)\right\} + \frac{2}{3r}\frac{\partial}{\partial r}\left\{\mu r\left(2\frac{\partial v}{\partial r}-\frac{\partial u}{\partial x}-\frac{v}{r}\right)\right\} + \frac{2\mu}{3r}\left(\frac{\partial u}{\partial x}+\frac{\partial v}{\partial r}-\frac{2v}{r}\right)\right] \quad (3b)$$

Energy equation for gas

Table 1
Simulation conditions used for the MCVD process with $SiCl_4$ and $GeCl_4$

E_{SC} (J mol^{-1})	4.02×10^5
E_{GC} (J mol^{-1})	2.63×10^5
ΔH_{SC} (J mol^{-1})	2.51×10^5
ΔH_{GC} (J mol^{-1})	4.6×10^4
$k_{SC,0}$ (s^{-1})	1.7×10^{14}
$k_{SC,1}$ (m^3 mol^{-1} s^{-1})	3.1×10^{13}
$k_{GC,0}$ (m^3 mol^{-1} s^{-1})	2.3×10^9
v_0[a]	1.39×10^{-9}
k_0, k_1, k_2[b]	4.52×10^{-3}, 7.62×10^{-5}, -9.80×10^{-9}
$C_{p,0}$, $C_{p,1}$, $C_{p,2}$[c]	7.16, 1.0×10^{-3}, -0.4×10^5
$D_{SC,0}$, $D_{GC,0}$, $D_{CL,0}$[d]	6.32×10^{-10}, 6.0×10^{-10}, 1.12×10^{-9}

[a] $v = v_0 T^{1.64874}$.
[b] $k = k_0 + k_1 T + k_2 T^2$.
[c] $C_p = C_{p,0} + C_{p,1} T + C_{p,2} T^{-2}$.
[d] $D_i = D_{i,0} T^{1.6561}$.

$$CC_p\left(\frac{\partial T}{\partial t} + v\frac{\partial T}{\partial r} + u\frac{\partial T}{\partial x}\right) = \frac{1}{r}\frac{\partial}{\partial r}\left(kr\frac{\partial T}{\partial r}\right) + \frac{\partial}{\partial x}\left(k\frac{\partial T}{\partial x}\right) + r_{SC}\Delta H_{SC} + r_{GC}\Delta H_{GC} \quad (4)$$

Energy equation for quartz tube

$$\rho C_p\frac{\partial T}{\partial t} = \frac{1}{r}\frac{\partial}{\partial r}\left(kr\frac{\partial T}{\partial r}\right) + \frac{\partial}{\partial x}\left(k\frac{\partial T}{\partial x}\right) \quad (5)$$

Species equations

$$C\left(\frac{\partial X_i}{\partial t} + v\frac{\partial X_i}{\partial r} + u\frac{\partial X_i}{\partial x}\right) = \frac{1}{r}\frac{\partial}{\partial r}\left(CD_i r\frac{\partial X_i}{\partial r}\right) + \frac{\partial}{\partial x}\left(CD_i\frac{\partial X_i}{\partial x}\right) + S_i \quad (6)$$

where ΔH_i represents the reaction enthalpy of oxidation of species i ($SiCl_4$, $GeCl_4$) and X_i and D_i denote mole fraction and diffusion coefficient of species i ($SiCl_4$, $GeCl_4$, Cl_2), respectively. The source term S_i in species equation is expressed as

$$S_{SC} = -r_{SC}, \quad S_{GC} = -r_{GC}, \quad S_{CL} = 2r_{SC} + 2r_{GC} \quad (7)$$

Kim and Pratsinis [11] and Powers [16] suggested the following equations for r_{SC} and r_{GC}

$$r_{SC} = (k_{SC,0} + k_{SC,1} C X_{O2})\exp(-E_{SC}/R_G T) C X_{SC} \quad (8)$$

$$r_{GC} = k_{GC,0}\exp(-E_{GC}/R_G T) C^2 (X_{GC} X_{O2} - \gamma Y_{GO} X_{CL}^2/K_{EQ}) \quad (9)$$

where the particle phase is assumed to be an ideal solution ($\gamma = 1$) and particle surface reaction is assumed to be negligible.

Since relatively dilute suspensions in an excess oxygen flow are employed, the mixture gas properties are calculated as properties of the carrier gas, O_2. These are given as a function of T and p using literature expressions for viscosity and diffusion [18], heat capacity [19] and thermal conductivity [20]. The details are summarized in Table 1.

The particle size of SiO_2 and GeO_2 is O (0.1 μm). Thus, diffusion is negligible compared with thermophoresis and bulk gas motion [2,3]. The mass balance equation for SiO_2 and GeO_2 are written as

$$C\frac{\partial n_i}{\partial t} + C[(\vec{V} + \vec{V}_T)\cdot\nabla]n_i = r_i \quad (10)$$

where $\vec{V}_T$ denotes the thermophoretic velocity defined by $\vec{V}_T = -K(\nu/T)\nabla T$ [21] and n_is are moles of species i particles per mole of carrier gas. The boundary conditions are

$$x = 0,\ r \le R_i\text{: } u = 2u_0[1 - (r/R_i)^2],\ v = 0,\ T = T_0,\ X_{SC} = X_{SC,0},\ X_{GC} = X_{GC,0},\ X_{CL} = 0;\ n_{SO} = n_{GO} = 0 \quad (11)$$

$$x = 0,\ R_i < r \le R_o\text{: } \frac{\partial T}{\partial x} = 0 \quad (12)$$

$$x = L,\ r \le R_i\text{: } \frac{\partial^2(u,v,T,X_{SC},X_{GC},X_{CL})}{\partial x^2} = 0 \quad (13)$$

$$x = L,\ R_i < r \le R_o\text{: } \frac{\partial T}{\partial x} = 0 \quad (14)$$

$$r = 0\text{: } \frac{\partial(u,v,T,X_{SC},X_{GC},X_{CL},n_{SO},n_{GO})}{\partial r} = 0 \quad (15)$$

$$r = R_i\text{: } u,\ v = 0,\ \frac{\partial(X_{SC},X_{GC},X_{CL})}{\partial r} = 0 \quad (16)$$

and continuity of temperature and heat flux

The localized heating by the torch is modeled as Gaussian distribution and dissipated by convection and radiation at the outer tube wall [12];

$$r = R_o\text{: } q_{max}\exp[-\lambda^2(x - x_{torch})^2] = k\frac{\partial T}{\partial r} + h(T - T_\infty) + \varepsilon\sigma(T^4 - T_\infty^4) \quad (17)$$

where x_{torch} is the torch location and h is the temperature-dependent heat transfer coefficient on the rotating

cylinder [22]. Two parameters, λ and q_{max}, control the width and the maximum value of the heating profile [12]. The emissivity of the quartz tube, ε, is calculated from a band approximation [23], with the assumption that the quartz is transparent below 4.5 μm wavelength and behaves like a black body above that.

In studies of optical fiber drawing, Homsy and Walker [24] and Paek and Runk [25] considered the effect of radiation in a silica solid rod by using the Rosseland diffusion approximation [23]. The same approximation is utilized in the present study:

$$k = k_{cond} + k_{rad} = k_{cond} + 16n^2\sigma T^3/3\alpha \quad (18)$$

where the Rosseland mean absorption coefficient, α and the refractive index, n, take the values of 4 and 1.5 cm^{-1}, respectively [24,25].

The above set of governing equations subject to the given boundary conditions were solved in terms of the primitive variables by employing the finite volume technique along with power law scheme and SIMPLE algorithm [26]. The pressure correction equation is solved with the MCGS solver [27] and other discretized equations are solved with CGS solver [28]. Convergence is assumed when the summed residual over the domain falls below a prescribed tolerance (10^{-3}). More stringent convergence criteria did not reveal noticeable changes in the solution. After the solution converges, the deposition masses of SiO_2 and GeO_2 per unit area at a certain axial location are evaluated from the mass fluxes onto the inner surface of tube, as follows:

$$\delta m_i(x,t) = \int_0^t (-CM_i n_i K v \partial \ln T/\partial r)_{r=R_i} d\tilde{t} \quad (19)$$

The deposition thicknesses for fully sintered particle layers can be obtained by dividing δm_i by the solid density of SiO_2 and GeO_2.

The grids near the reaction zone should be denser due to steep changes resulting from the chemical reaction. Therefore, non-uniform grids are generated each time step with the torch movement. From the preliminary grid sensitivity test, grid spaces chosen are maximum axial grid space, $\Delta x_{max} = 5$ mm, minimum axial grid space, $\Delta x_{min} = 1$ mm, radial grid space, $\Delta r = 0.7$ mm and time interval, $\Delta t = 1$ s. Deposition masses of SiO_2 and GeO_2 in this grid system differ from the denser grid system ($\Delta x_{max} = 2.5$ mm, $\Delta x_{min} = 0.5$ mm, $\Delta r = 0.7$ mm and $\Delta t = 1/3$ s) by less than 3 and 4%, respectively.

3. Results and discussion

In order to make a proper assessment of our numerical implementation, the previous numerical and experimental studies for single component SiO_2 deposition [14,15] have been compared with the present calculations. The in-take flow rate of carrier gas, O_2, is 2 l min^{-1} and the flow rate of $SiCl_4$ and $GeCl_4$ is 3 and 1.9 mol m^{-3} (Table 1). Since overall efficiency can be expressed as a function of minimum temperature [3], a proper prediction of wall temperature is a prerequisite condition for a correct estimation of efficiency. Fig. 2 shows the spatial wall temperature variation at several different times (i.e. different torch locations) using the relative coordinate that moves with the torch, $x_{rel} = (x - x_{torch})$. Reasonably good agreement was obtained compared with quasi-steady experiments [14] at later times (i.e. larger distance of torch movement). However, at early times, the discrepancies between the present unsteady and previous quasi-steady calculations are shown to be significant, which indicates the importance of unsteady analysis, especially at early times. It is also noted that the previous calculation considering only the effect of $SiCl_4$ oxidation agrees very well with the present calculation considering both chemical reactions of $SiCl_4$ and $GeCl_4$. Therefore, the effect of $GeCl_4$ reaction on the wall temperature would be small. The dashed and solid lines represent temperature distributions for the first pass and second pass of the torch traverse, respectively. The wall temperature ahead of the torch for the second pass is higher than that of the first pass and there exists an axial region where the wall temperature increases ahead of the torch. This is a consequence of the residual heat from the first pass. This temperature increase coincides with experiment [14] and was also predicted by a two-torch quasi-steady model suggested by Park and Choi [12]. At early times, wall temperature distributions in the region behind the torch do not fall onto a single curve even when they are plotted using the relative moving coordinate, x_{rel} and are much different from quasi-

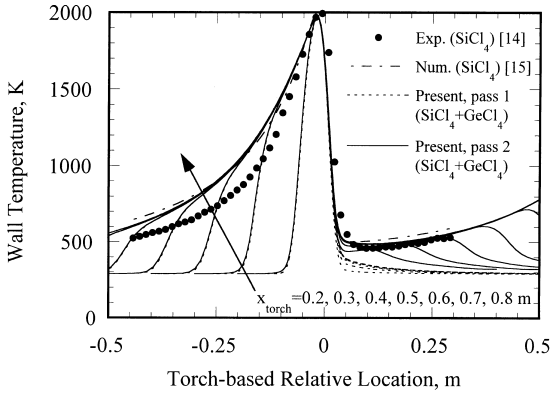

Fig. 2. Distribution of tube wall temperature with respect to the torch based relative axial coordinate for different torch locations (different times).

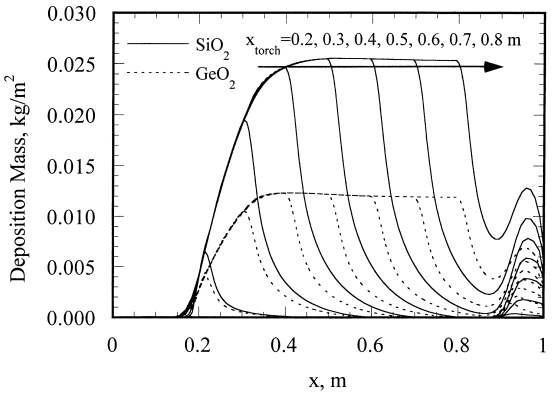

Fig. 3. Deposition profiles of SiO_2 and GeO_2 with respect to torch traversing.

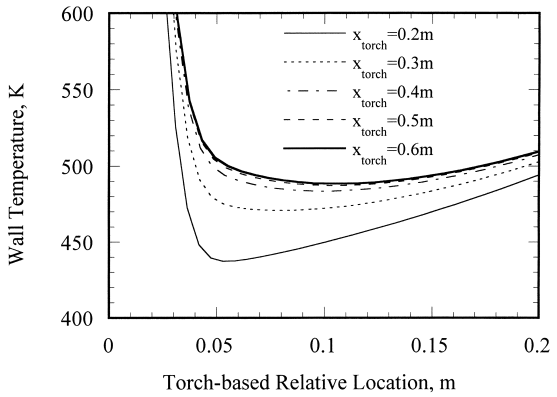

Fig. 5. The variations of minimum wall temperature for different torch locations (different times).

steady results. This means that the quasi-steady assumption is not valid at early times. We also note that previous discrepancies in the deposition profile between quasi-steady state predictions and measurements near the inlet region were significantly improved by using a full unsteady calculation for the case of single component SiO_2 particle deposition [15]. It is now extended to consider the unsteady heat and mass transfer for multi-component SiO_2 and GeO_2 particle deposition.

Fig. 3 shows the deposition mass profiles of SiO_2 and GeO_2 for the constant torch speed case. Note the axially non-uniform deposition for both SiO_2 and GeO_2 deposition near the entry. Since this tapered entry must be eliminated before drawing the preform of optical fiber, it is desirable to reduce the tapered length. Therefore, there is a great need to find out the operating condition reducing this non-uniform deposition of multi-component SiO_2/GeO_2 particles.

Fig. 4 shows the thermophoretic flux to the wall, defined as $\vec{V}_T C n_i$. $\vec{V}_T$ is the thermophoretic particle velocity and C and n_i are gas concentration and moles of species SiO_2 and GeO_2 per mole of carrier gas. The deposition efficiency is low at the beginning of torch traverse compared to when torch moves enough to reach steady state. At the beginning of torch traverse, the narrow region of high wall temperature (shown in Fig. 2) causes this low deposition efficiency. Note that there is a maximum deposition efficiency at $x_{\text{travel}} = 0.3$ m before it reaches steady state. The decrease of deposition efficiency beyond $x_{\text{travel}} = 0.3$ m is due to the increase of the minimum wall temperature ahead of the torch. Fig. 5 shows the wall temperature distribution ahead of the torch for different torch travel locations (or different times). The minimum wall temperature is about 435 K at the beginning of torch traverse and becomes steady near 500 K as the torch moves on. The effects of exothermic chemical reactions would cause the increase of the minimum wall temperature as the torch travels and a similar effect was observed experimentally [14]. As the wall temperature becomes higher, the particle deposition is suppressed due to lower thermophoretic particle velocity. On the other hand, as the torch moves on, particle formation in a tube becomes more active, which would tend to increase the deposition flux. Therefore, there are two mechanisms of which each has the opposite effect: the increasing minimum temperature to reduce the deposition flux and the increasing particle formation to increase the deposition flux. Correspondingly, the maximum deposition flux may exist as the torch moves. Note also that the broad range of particle deposition occurs, which should cause the undesirable tapered entry. This means that there would be the area of non-uniform deposition that is equivalent to the broad particle deposition area, even if quasi-steady state is reached.

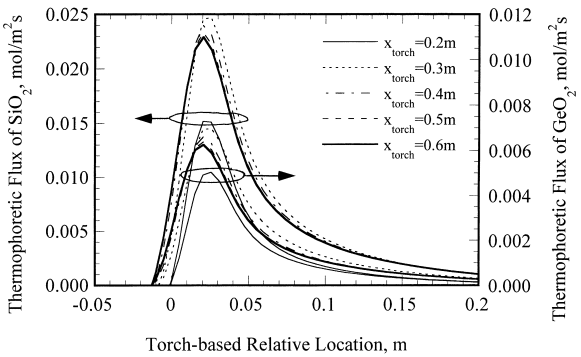

Fig. 4. Thermophoretic fluxes of SiO_2 and GeO_2 to the tube wall for different torch locations (different times).

Torch speed control was shown to be effective to result in a much shorter tapered entry for single com-

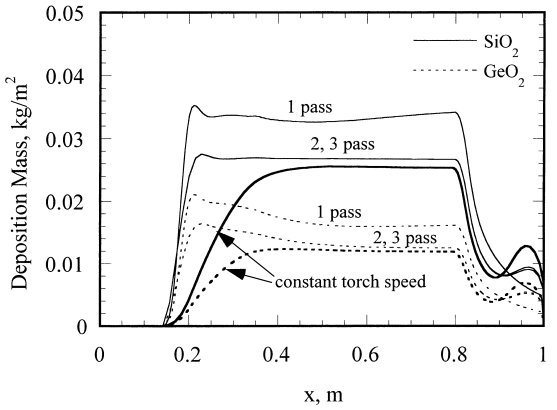

Fig. 6. Comparison of the deposition profiles of SiO_2 and GeO_2 between cases of variable torch speed (thin lines) and constant torch speed (bold lines).

ponent SiO_2 deposition than the constant torch speed case [15]. This may be also true for multi-component SiO_2/GeO_2 particle deposition. To examine the validity of torch speed variation on the enhancement of deposition performance, calculations with the same torch speed variation utilized previously in single component SiO_2 deposition [15], which is linearly increased up to 120 s and then maintains at 0.2 m/min, have been done for the multi-component particle deposition case. Fig. 6 shows the deposition profiles of SiO_2 and GeO_2 during three passes. The deposition masses of both SiO_2 and GeO_2 during the first pass are more than those during the second or third pass because the minimum wall temperatures of the latter are approximately 200 K higher than the former, due to the heat remaining from the first pass. There is no difference between second and third passes, which indicates calculations for further passes are not necessary. For SiO_2 deposition, the uniformity has been much improved compared to the case of constant torch speed (bold solid line) as already confirmed by Park and Choi [15]. The reason for this improvement was that the deposited mass near the torch starting position increased due to the longer duration of torch heating for the case of linearly varying torch speed and thus the tapered entry region was greatly reduced by less than 0.1 m. The uniformity of deposition of GeO_2, however, becomes worse by the excessive particle deposition at the beginning. Note that for the constant torch speed case, the deposition of GeO_2 becomes steady earlier ($x \approx 0.35$ m) than SiO_2 ($x \approx 0.45$ m) shown in Fig. 3, because the activation energy of $GeCl_4$ oxidation is lower than that of $SiCl_4$ oxidation. Therefore, the strategy of slowing down the torch speed for the enhancement of SiO_2 uniformity may cause excessive particle deposition of GeO_2 over a broad zone. Thus, the different characteristics in chemical reactions between $SiCl_4$ and $GeCl_4$ pose a difficulty in achieving both uniformity of SiO_2 and GeO_2 simultaneously by the use of only one control method, e.g. the variation of torch speed in time.

To ensure the uniformity of both SiO_2 and GeO_2, a control strategy may need the variation of at lease two parameters, rather than changing only one parameter. For this purpose, parametric studies have been conducted varying three operating parameters over time, i.e. maximum wall temperature, torch speed and intake amount of $GeCl_4$, independently or varying a set of two parameters simultaneously. The conditions for the base case are $T_{max} = 1973$ K, $V_{torch} = 0.2$ m min^{-1} and $C_{GC,0} = 1.9$ mol m^{-3}. Case A is the variation of torch speed which is linearly increased from zero to 0.2 m min^{-1} for 120 s and then maintains uniform as 0.2 m min^{-1} after 120 s. Case B is similar to case A, except for beginning the torch speed with an initial torch speed, 0.0667 m min^{-1}. Case C and D are variations of maximum wall temperatures with the same torch speed variation as case A. Case C lowers the maximum wall temperature from T_0 by about 50°C as

Table 2
Parametric studies for searching optimum operating parameters of time dependent maximum wall temperature, torch speed and intake amount of $GeCl_4$[a]

	T_{max} (K)	V_{torch} (m min^{-1})	$C_{SC,0}$ (mol m^{-3})	$C_{GC,0}$ (mol m^{-3})
Base	T_{max}	V_0	C_1	C_2
A	T_{max}	$\min[V_0 t/t_0, V_0]$	C_1	C_2
B	T_{max}	$\min[V_0(2t/t_0+1)/3, V_0]$	C_1	C_2
C	$-a_T(x_{travel}/x_{sweep}) + T_{max}$	$\min[V_0 t/t_0, V_0]$	C_1	C_2
D	$a_T(x_{travel}/x_{sweep}-1) + T_{max}$	$\min[V_0 t/t_0, V_0]$	C_1	C_2
E	T_{max}	$\min[V_0 t/t_0, V_0]$	C_1	$a_x(x_{travel}/x_{sweep}-1) + C_2$
F	T_{max}	$\min[V_0 t/t_0, V_0]$	C_1	$b_x x_{travel}/x_{sweep} + C_2$

[a] $T_{max} = 1973$ K, $a_T = 50$ K, $x_{sweep} = 0.75$ m, $t_0 = 120$ s, $V_0 = 0.2$ m min^{-1}, $C_1 = 3$ mol m^{-3}, $C_2 = 1.9$ mol m^{-3}, $a_x = 0.475$ mol m^{-3}, $b_x = 0.665$ mol m^{-3}.

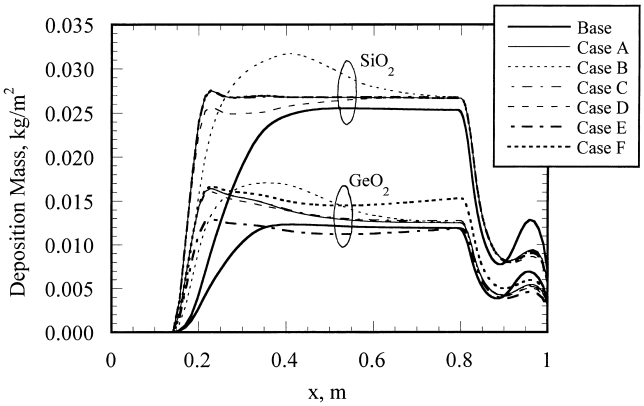

Fig. 7. Deposition profiles of SiO_2 and GeO_2 corresponding to the various operating parameters in Table 2.

the torch travels, while case D raises the maximum wall temperature by about 50°C from 1923 K at the starting position. Case E and F represent time dependent variations of in-take amount of $GeCl_4$, which is linearly increased. The details on the variations of parameters used for each case are summarized in Table 2.

Fig. 7 shows the deposition profiles of SiO_2 and GeO_2 for seven different cases. In case A, the enhancement of deposition uniformity of SiO_2 is quite clear compared with the base case but the deterioration of deposition uniformity of GeO_2 is also found, as mentioned earlier. Slight change of torch speed profile (case B) makes it worse for the uniformity of both SiO_2 and GeO_2. Thus hereafter the torch speed variation is fixed with that of case A and then the change of another parameter has been studied to find uniform deposition of GeO_2 and SiO_2. The effect of lowering the maximum wall temperature (case C) by 50°C would be negligible and resulted in almost the same depositions as case A. Case D has been carried out to examine that lower maximum wall temperature at the starting position may reduce the reaction rate of $GeCl_4$ and decrease the deposition amount of GeO_2 at entry region where excessive deposition was made for case A. This has a positive effect to some extent for the deposition uniformity of GeO_2. However, the low maximum wall temperature also reduces the reaction rate of $SiCl_4$ and makes the non-uniform deposition profile of SiO_2 near the entry region. Both cases E and F, where the in-take amount of $GeCl_4$ is linearly increased to suppress the initial high deposition of GeO_2, yielded considerable enhancement of deposition uniformity on both SiO_2 and GeO_2, while case F resulted not only in uniform GeO_2 deposition, but also a higher deposition rate than case E. Thus the uniformity of deposition thickness of SiO_2 can be maintained by torch speed variation over time and that of GeO_2 may be simultaneously obtained by increasing the in-take flow rate of $GeCl_4$ as the torch travels.

4. Conclusions

Unsteady heat and mass transfer analysis on the codeposition of SiO_2 and GeO_2 during the modified chemical vapor deposition process has been conducted. The present unsteady analysis has been shown to be an effective and versatile tool to examine the effects of the time dependent variations of different operating parameters on deposition performance for enhancement of uniform deposition profile and short tapered entry region.

The tapered entry region for SiO_2 deposition can be reduced by varying the torch speed in time, that is, linearly increasing speed up to a certain time and maintaining at constant speed beyond that time. However, this optimized torch speed, which was valid for SiO_2 deposition, resulted in the deterioration of GeO_2 uniformity. Therefore, to ensure the uniformity of both SiO_2 and GeO_2, a control strategy may need variations of at least two parameters, rather than changing only one parameter. Parametric studies varying three operating parameters over time, i.e. maximum wall temperature, torch speed and in-take amount of $GeCl_4$, independently or varying a set of two parameters simultaneously, have been conducted to find optimum operating conditions. The uniformity of deposition thickness of SiO_2 is obtained by linearly varying torch speed and at the same time, GeO_2 uniformity can be obtained by increasing the in-take flow rate of $GeCl_4$ over time.

Acknowledgements

Part of this work was funded by National CRI Cen-

ter for Nano Particle Control supported by the Ministry of Science and Technology, Korea.

References

[1] J.B. MacChesney, P.B. O'Connor, H.M. Presby, New technique for preparation of low loss and graded index optical fibers, Proc. IEEE 62 (1974) 1278–1279.

[2] P.G. Simpkins, S.G. Kosinski, J.B. MacChesney, Thermophoresis: the mass transfer mechanism in MCVD, J. Appl. Phys. 50 (1979) 5676–5681.

[3] K.L. Walker, F.T. Geyling, S.R. Nagel, Thermophoresis deposition of small particles in the modified chemical vapor deposition (MCVD) process, J. Am. Ceram. Soc. 63 (1980) 552–558.

[4] C.W. Wang, T.F. Morse, J.W. Cippola Jr., Laser induced natural convection and thermophoresis, ASME J. Heat Transfer 107 (1985) 161–167.

[5] T.F. Morse, D. DiGiovanni, Y.W. Chen, J.W. Cippola Jr., Laser enhancement of thermophoretic deposition process, J. Lightwave Technol. LT-4 (1986) 151–155.

[6] K.S. Kim, S.E. Pratsinis, Manufacture of optical waveguide preforms by MCVD, AIChE J. 34 (1988) 912–920.

[7] M. Fiebig, M. Hilgenstock, H.A. Rieman, The modified chemical vapor deposition process in a concentric annulus, Aerosol Sci. Technol. 9 (1988) 237–249.

[8] M. Choi, K.S. Park, Effects of annular jet in inside vapor deposition with applications to optical fiber manufacture, in: 10th International Heat Transfer Conference, vol. 7, 1994, pp. 209–214.

[9] M. Choi, Y.T. Lin, R. Greif, Analysis of buoyancy and tube rotation relative to MCVD process, ASME J. Heat Transfer 112 (1990) 1063–1069.

[10] Y.T. Lin, M. Choi, R. Greif, Three dimensional analysis of particle deposition for the modified chemical vapor deposition (MCVD) process, ASME J. Heat Transfer 114 (1992) 735–742.

[11] K.S. Kim, S.E. Pratsinis, Codeposition of SiO_2/GeO_2 during production of optical fiber preforms by modified chemical vapor deposition, Int. J. Heat Mass Transfer 33 (1990) 1977–1986.

[12] K.S. Park, M. Choi, Conjugate heat transfer and particle deposition process: effect of torch speed and solid layer, Int. J. Heat Mass Transfer 37 (1994) 1593–1603.

[13] S. Joh, R. Greif, The effects of $SiCl_4$ and $GeCl_4$ oxidation, variable properties, buoyancy and tube rotation on the Modified Chemical Vapor Deposition (MCVD) process, Int. J. Heat Mass Transfer 38 (1994) 1911–1921.

[14] J. Cho, M. Choi, An experimental study of heat transfer and particle deposition for the modified chemical vapor deposition, ASME J. Heat Transfer 117 (1995) 1036–1041.

[15] K.S. Park, M. Choi, Analysis of unsteady heat and mass transfer during the modified chemical vapor deposition process, ASME J. Heat Transfer 120 (1998) 858–864.

[16] D.R. Powers, Kinetics of $SiCl_4$ oxidation, J. Am. Ceram. Soc. 61 (1978) 295–297.

[17] D.L. Wood, K.L. Walker, J.B. MacChesney, J.R. Simpson, R. Csencsits, Germanium chemistry in the MCVD process for optical fiber fabrication, J. Lightwave Technol. LT-5 (1987) 277–285.

[18] R.C. Reid, J.M. Prausnitz, T.K. Sherwood, The Properties of Gases and Liquids, 3rd ed., McGraw-Hill, New York, 1977.

[19] J.M. Smith, H.C. Van Ness, Introduction to Chemical Engineering Thermodynamics, third ed., McGraw-Hill, New York, 1975.

[20] R.H. Perry, D. Green, Perry's Chemical Engineers' Handbook, 6th ed., McGraw-Hill, New York, 1984.

[21] L. Talbot, R.K. Cheng, R.W. Schefer, D.R. Willis, Thermophoresis particles in a heated boundary layer, J. Fluid Mech. 101 (1980) 737–758.

[22] B. Farouk, K.S. Ball, Convective flow around a rotating isothermal cylinder, Int. J. Heat Mass Transfer 28 (1985) 1921–1935.

[23] R. Siegel, J.R. Howell, Thermal Radiation Heat Transfer, 3rd ed., Hemisphere, Washington, DC, 1992.

[24] G.M. Homsy, K.L. Walker, Heat transfer in laser drawing of optical fibers, Glass Technol. 20 (1979) 20–26.

[25] U.C. Paek, R.B. Runk, Physical behavior of the neck-down region during furnace drawing silica fibers, J. Appl. Phys. 49 (1978) 4417–4423.

[26] S.V. Patankar, Numerical Heat Transfer and Fluid Flow, Hemisphere, Washington, DC, 1980.

[27] C.-J. Kim, S.T. Ro, Efficient and robust matrix solver for the pressure-corrections in flow problems, Numerical Heat Transfer 27B (1995) 355–369.

[28] D.S. Kershaw, The incomplete Cholesky-conjugate gradient method for the iterative solution of systems of linear equations, J. Comp. Phys. 26 (1978) 43–65.